Model_Title	Time period (ka)	*ADF* $_{median}$ (μT)	ADF_{iqr} (μT)	*NADF* $_{median}$ (μT)	$NADF_{iqr}$ (μT)	TF_{median} (μT)	TF_{iqr} (μT)	*Roughness*	*Volatility*	Reference
pfm9k.2	0-9	**46.4**	8.0	**8.5**	3.5	47.5	9.0	**0.43**	**0.44**	Nilsson et al., 2022
ArchKalmag14K	0-14	**50.0**	5.0	**9.0**	4.4	50.7	4.8	**0.42**	**0.31**	Schanner et al., 2022
LSMOD	30-50	**28.2**	12.5	**9.4**	3.6	30.1	11.8	**0.58**	**0.65**	Brown et al., 2018
GGFSS70	15-70	**29.7**	10.5	**7.8**	2.9	30.6	10.2	**0.51**	**0.59**	Panovska et al., 2021
GGF100k	0-100	**37.6**	8.0	**8.3**	2.8	38.4	8.0	**0.47**	**0.46**	Panovska et al., 2018
GGFMB	700-900	**27.3**	11.9	**10.5**	5.3	29.5	10.6	**0.62**	**0.62**	Mahgoub et al., 2023
TK03	0-5000	**25.5**	12.0	**7.1**	2.6	26.6	11.5	**0.53**	**0.67**	Tauxe and Kent, 2004
BB18	0-10000	**31.1**	20.5	**9.5**	3.4	32.7	19.5	**0.55**	**0.79**	Bono et al., 2020
BB18z3	0-10000	**31.4**	20.3	**9.8**	3.4	33.1	19.3	**0.56**	**0.78**	Bono et al., 2020
THG24	0-10000	**25.2**	11.8	**6.9**	2.4	26.2	11.3	**0.52**	**0.67**	Tauxe et al., 2024
BBM22	5000-23000	**21.1**	18.7	**6.0**	2.1	22.1	17.8	**0.53**	**0.92**	Engbers et al., 2022

Table S1: Summary of geomagnetic field models used in this study including Spherical Harmonic Analogues (in bold)

Simulation	Buoyancy	*E*	*Pr*	*Pm*	*q**	*Ra*	E_m/E_k	*Rm*	Duration (kyr)	Timestep (kyr)	f_{dip}	ΔQ_{PM}	*ADF* $_{median}$ (μT)	ADF_{iqr} (μT)	*NADF* $_{median}$ (μT)	$NADF_{iqr}$ (μT)	TF_{median} (μT)	TF_{iqr} (μT)	*Roughness*	*Volatility*	Reference
THOM1-1.5	T					150	2.5	107	3426	0.090	0.84	11.0	**54.2**	13.7	**8.5**	3.9	55.0	13.8	**0.39**	**0.51**	
THOM1-2	T					200	3.4	121	5688	0.398	0.75	9.3	**48.0**	7.3	**9.3**	3.2	49.0	7.5	**0.44**	**0.39**	
THOM1-3	T					300	3.0	148	5110	0.399	0.7	8.6	**55.7**	7.1	**11.8**	3.4	57.1	7.2	**0.46**	**0.36**	
THOM1-4	T	1.5×10^{-4}	1	3	0	400	2.3	176	4345	0.399	0.69	8.5	**55.1**	7.2	**11.5**	3.3	56.4	7.2	**0.46**	**0.36**	Biggin et al.(2025)
THOM1-8	T					800	1.2	262	4007	0.399	0.63	6.9	**48.5**	8.0	**11.8**	3.6	50.1	8.0	**0.49**	**0.41**	
THOM1-12	T					1200	0.8	333	3156	0.400	0.57	4.4	**40.6**	15.0	**11.1**	4.4	42.2	15.3	**0.52**	**0.61**	
THOM1-17.5	T					1750	0.2	724	765	0.120	0.15	18.5	**3.2**	4.3	**6.3**	2.1	7.5	3.1	**1.42**	**0.99**	
THET1-1.2	T					120	4.6	94	709	0.101	0.79	9.7	**40.6**	16.3	**6.4**	5.4	41.3	17.3	**0.40**	**0.65**	
THET1-1.5	T					150	4.6	104	2393	1.456	0.77	9.1	**42.0**	12.1	**7.8**	4.2	42.9	12.7	**0.43**	**0.55**	
THET1-2	T					200	4.5	115	2673	1.034	0.66	7.7	**49.6**	7.7	**12.3**	4.6	51.2	8.4	**0.50**	**0.41**	
THET1-2.5	T					250	3.8	148	708	0.286	0.64	7.8	**50.1**	8.5	**13.2**	4.2	52.1	9.0	**0.51**	**0.42**	
THET1-3.5	T					350	2.6	156	1230	0.204	0.63	7.6	**47.2**	6.1	**12.6**	3.7	49.1	6.2	**0.52**	**0.36**	
THET1-5	T	1.5×10^{-4}	1	3	2.3	500	1.8	205	1718	0.026	0.61	7.4	**42.8**	8.0	**11.5**	3.3	44.6	8.2	**0.52**	**0.44**	Biggin et al.(2025)
THET1-7.5	T					750	0.9	288	795	0.469	0.56	7.0	**30.0**	8.3	**9.5**	3.3	31.5	8.9	**0.56**	**0.55**	
THET1-8*	T					800	0.9	274	182	0.019	0.53	6.9	**30.6**	14.0	**9.8**	5.3	32.2	14.7	**0.57**	**0.69**	
THET1-12*	T					1200	0.6	340	795	0.007	0.5	7.2	**25.9**	11.8	**9.0**	4.1	27.4	12.4	**0.59**	**0.69**	
THET1-17.25*	T					1725	0.5	389	836	0.203	0.46	7.3	**21.7**	10.0	**9.0**	4.1	23.7	10.1	**0.64**	**0.68**	
THET1-24.15	T					2415	0.3	496	804	0.151	0.38	6.4	**14.9**	12.1	**8.4**	4.2	17.8	11.9	**0.75**	**0.89**	
TCHET1-1.5	TC					150	1.7	125	771	0.105	0.82	12.4	**35.6**	2.9	**4.9**	1.5	36.0	3.0	**0.37**	**0.29**	
TCHET1-2	TC					200	1.6	146	870	0.084	0.78	11.1	**37.3**	3.7	**5.6**	1.9	37.7	3.7	**0.39**	**0.32**	
TCHET1-3	TC					300	1.1	185	983	0.064	0.72	9.4	**35.1**	5.0	**6.7**	2.2	35.8	5.1	**0.44**	**0.38**	
TCHET1-5	TC	1.5×10^{-4}	1	3	2.3	500	0.8	244	497	0.053	0.64	7.8	**31.1**	8.0	**7.7**	2.7	32.1	8.2	**0.50**	**0.51**	Biggin et al.(2025)
TCHET1-7.5	TC					750	0.6	306	432	0.033	0.57	7.0	**26.6**	8.8	**7.9**	3.0	27.7	8.7	**0.55**	**0.57**	
TCHET1-10	TC					1000	0.5	357	490	0.086	0.48	7.4	**19.0**	11.0	**8.6**	3.0	20.7	10.3	**0.68**	**0.74**	
TCHET1-12	TC					1200	0.4	398	385	0.014	0.41	6.4	**16.3**	13.2	**7.7**	3.8	18.0	12.6	**0.69**	**0.88**	
THOM2-20	T	1×10^{-5}	0.2	1	0	2000	2.2	889	121	0.002	0.71	9.8	**86.0**	13.8	**17.9**	5.5	88.0	14.0	**0.46**	**0.40**	Mound & Davies (2023)
THOM2-60	T					6000	0.4	1848	127	0.002	0.19	15.5	**5.5**	6.9	**7.5**	2.5	9.9	4.7	**1.17**	**0.92**	
THET2-20	T	1×10^{-5}	0.2	1	2.3	2000	2.7	851	116	0.002	0.64	7.4	**82.2**	13.4	**19.1**	7.6	84.4	13.7	**0.48**	**0.41**	Mound & Davies (2023)
THET2-60	T					6000	0.9	1608	131	0.001	0.66	7.7	**60.6**	14.3	**11.6**	3.6	61.7	14.0	**0.44**	**0.48**	
THET3-20	T	1×10^{-5}	0.2	1	5	2000	3.5	830	53	0.001	0.54	6.2	**79.0**	12.3	**27.1**	9.1	83.4	12.9	**0.59**	**0.40**	Mound & Davies (2023)
THET3-60	T					6000	1.4	1483	91	0.001	0.63	5.6	**68.3**	31.8	**15.3**	7.7	70.3	32.6	**0.47**	**0.69**	
CHOM1-3.75	C					750	1.8		3400	0.035	0.83	12.6	**45.0**	8.0	**6.0**	2.0	45.4	8.0	**0.36**	**0.42**	
CHOM1-15	C					1500	0.7	281	12161	0.134	0.65	6.7	**44.2**	9.0	**11.6**	4.4	45.8	9.3	**0.51**	**0.46**	
CHOM1-22.5	C					2250	0.5	350	7114	0.145	0.56	3.3	**35.4**	14.1	**11.0**	5.0	37.3	14.5	**0.56**	**0.64**	
CHOM1-24*	C	1.5×10^{-4}	1	3	0	2400	0.4		7713	0.224	0.52	2.7	**30.7**	16.1	**10.1**	5.2	32.4	16.6	**0.57**	**0.74**	Meduri et al. (2021)
CHOM1-24.75*	C					2475	0.4	376	4484	0.137	0.48	2.8	**25.1**	18.1	**9.2**	5.0	26.9	18.2	**0.61**	**0.85**	
CHOM1-25.5*	C					2550	0.4	380	6215	0.135	0.47	3.5	**25.2**	20.5	**9.3**	5.6	27.0	20.4	**0.61**	**0.90**	
CHOM1-27	C					2700	0.3	395	8129	0.129	0.41	4.7	**17.7**	22.7	**8.1**	5.2	19.9	22.2	**0.67**	**1.12**	
CHOM1-30	C					3000	0.3	418	2205	0.122	0.37	6.9	**13.9**	20.1	**7.5**	5.1	16.2	19.4	**0.73**	**1.18**	
CHOM2-2.5	C					250	4.6	229	11613	0.138	0.58	6.5	**114.6**	14.7	**37.0**	11.1	120.9	15.2	**0.57**	**0.36**	
CHOM2-4	C					400	2.5	312	12074	0.106	0.51	5.4	**87.9**	22.6	**31.2**	11.6	93.7	23.9	**0.60**	**0.52**	
CHOM2-5	C					500	1.4	372	7155	0.113	0.44	4.9	**57.8**	20.9	**24.0**	9.3	62.9	21.7	**0.64**	**0.61**	
CHOM2-5.5	C	5×10^{-4}	1	10	0	550	1.0	401	11667	0.109	0.40	4.6	**44.7**	21.5	**20.8**	9.0	49.7	22.3	**0.68**	**0.71**	Meduri et al. (2021)
CHOM2-6.25	C					625		442	86271	1.241	0.32	5.6	**28.6**	23.7	**17.2**	8.4	33.8	23.1	**0.78**	**0.90**	
CHOM2-7.5	C					750		491	1869	0.098	0.26	8.7	**19.5**	21.2	**16.5**	8.2	26.2	19.1	**0.92**	**0.99**	
CHOM2-10	C					1000		564	4995	0.094	0.20	15.5	**11.2**	13.7	**18.3**	8.3	23.2	12.2	**1.28**	**1.04**	
THOM3-0.7	T					70	8.2		1659	0.097	0.62	5.0	**123.6**	30.1	**40.0**	14.4	130.8	30.6	**0.57**	**0.50**	
THOM3-0.75	T					75	7.2		1882	0.483	0.62	4.8	**120.8**	40.7	**36.7**	13.1	127.5	40.8	**0.55**	**0.58**	
THOM3-0.9	T					90	6.2		2308	0.429	0.61	5.1	**118.7**	34.6	**36.4**	14.8	125.2	35.3	**0.55**	**0.55**	
THOM3-1	T	5×10^{-4}	1	10	0	100	5.8	205	1440	0.013	0.62	5.9	**86.1**	18.6	**26.7**	8.9	90.3	18.7	**0.56**	**0.47**	Meduri et al. (2021)
THOM3-1.5*	T					150	1.8		6206	0.399	0.45	4.0	**39.6**	24.1	**16.4**	7.5	43.1	24.7	**0.64**	**0.79**	
THOM3-2.5	T					250	1.0		996	0.064	0.37	6.4	**29.9**	12.7	**15.3**	6.1	33.9	12.9	**0.72**	**0.66**	
THOM3-3.5	T					350	0.9	479	933	0.035	0.29	8.2	**22.6**	24.5	**15.8**	7.5	28.6	20.6	**0.84**	**0.95**	
THOM3-4.5	T					450	0.9	537	984	0.020	0.26	11.0	**16.7**	18.4	**18.2**	8.5	26.5	15.3	**1.04**	**0.96**	
CHOM3-30	C					300		264	2132	0.174	0.68	9.3	**50.5**	7.8	**9.8**	2.9	51.6	7.8	**0.44**	**0.39**	
CHOM3-45	C	1.5×10^{-4}	1	3	0	450		340	7328	0.128	0.61	6.3	**35.4**	11.6	**8.6**	3.3	36.7	11.8	**0.49**	**0.58**	Meduri et al. (2021)
CHOM3-90	C					900		497	1569	0.086	0.27	8.7	**8.3**	9.6	**7.0**	2.8	11.4	7.7	**0.92**	**0.97**	

Table S2: Summary of input and output values of published geodynamo simulations used as the ensemble for SHAnalogue estimation. Bold, asterisked simulations are those with *Roughness* and *Volatility* values within bounds of estimates from 4-15 Ma. Buoyancy refers to the driving as (T)hermal, (TC)thermochemical, or (C)hemical. *E* is the Ekman number; *Pr* is the Prandtl number; *Pm* is the magnetic Prandtl number; *q** measures heterogeneity in heat flow on the outer boundary following a pattern based on seismic tomography of the lowermost mantle (Masters et al., 1996). *Ra* is Rayeigh number; E_m/E_k is the ratio of the magnetic to kinetic energies; *Rm* is the magnetic Reynolds number. Durations and timesteps were calculated assuming a magnetic diffusion time of 200 kyr. Parameter f_{dip} is time-average dipolar fraction of the field at the core-mantle boundary (Christensen & Aubert, 2006); ΔQ_{PM} is the misfit produced by the realistion to the criteria of Sprain et al. (2019). Other terms are SHAnalogues (in bold) or related parameters defined in text. Entries are blank if information is not available. For full descriptions of all simulations, see the associated references.

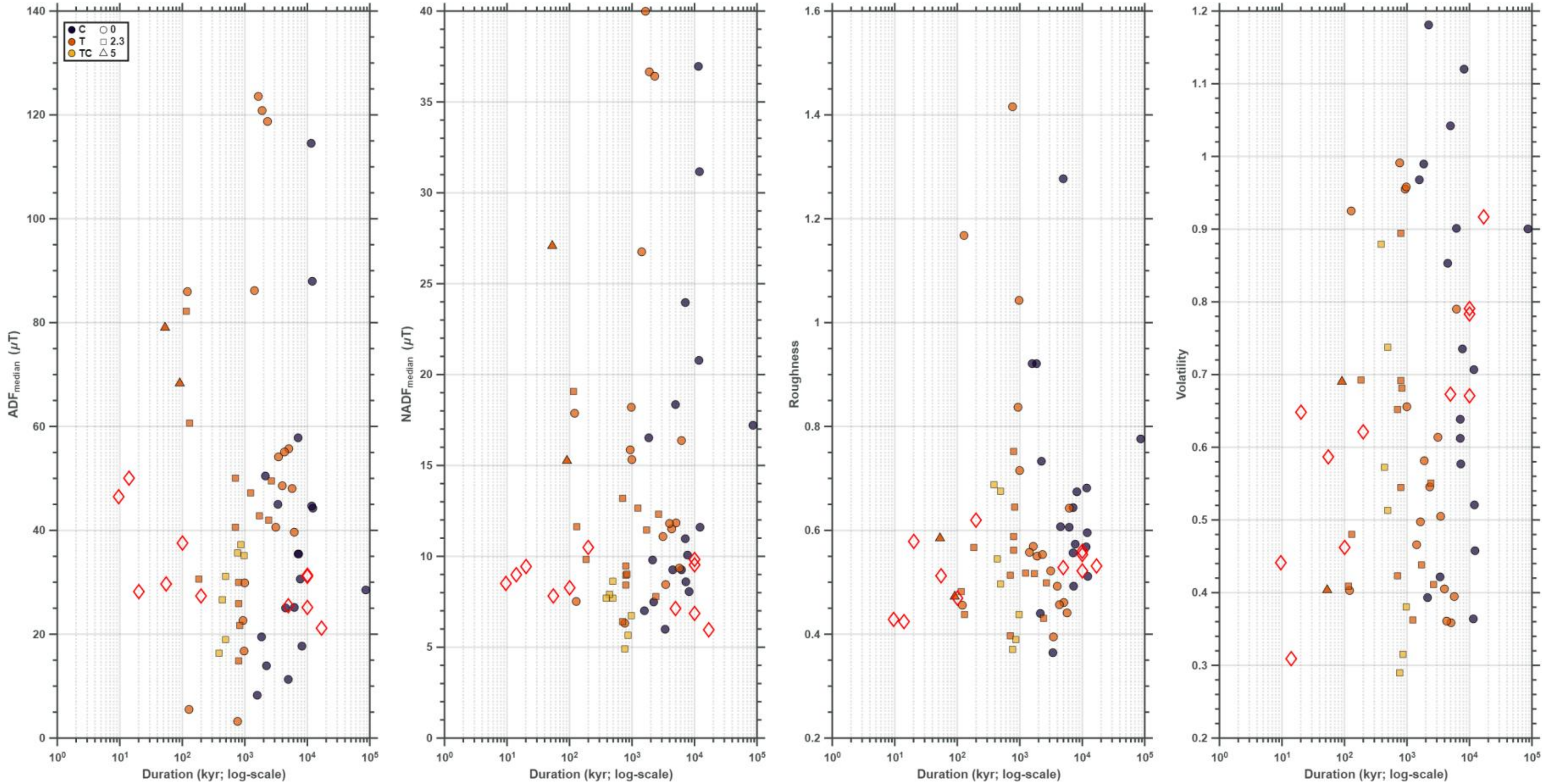

Figure S1: Summary of spherical harmonic analogues of field models (see Table S1) and geodynamo simulations (Table S2) used in this study plotted versus the durations of the realisations. Geomagnetic field models are shown as large red diamonds. Colours and shapes of points representing geodynamo simulations are set, respectively, according to their buoyancy source ((C)hemical; (T)hermal; (TC)thermochemical) and the magnitude of the thermal heterogeneity imposed on their outer boundaries (defined by q^*, Mound & Davies, 2023), A legend is given in panel (a). The duration of geodynamo simulation was scaled assuming a magnetic diffusion timescale of 200 kyr.

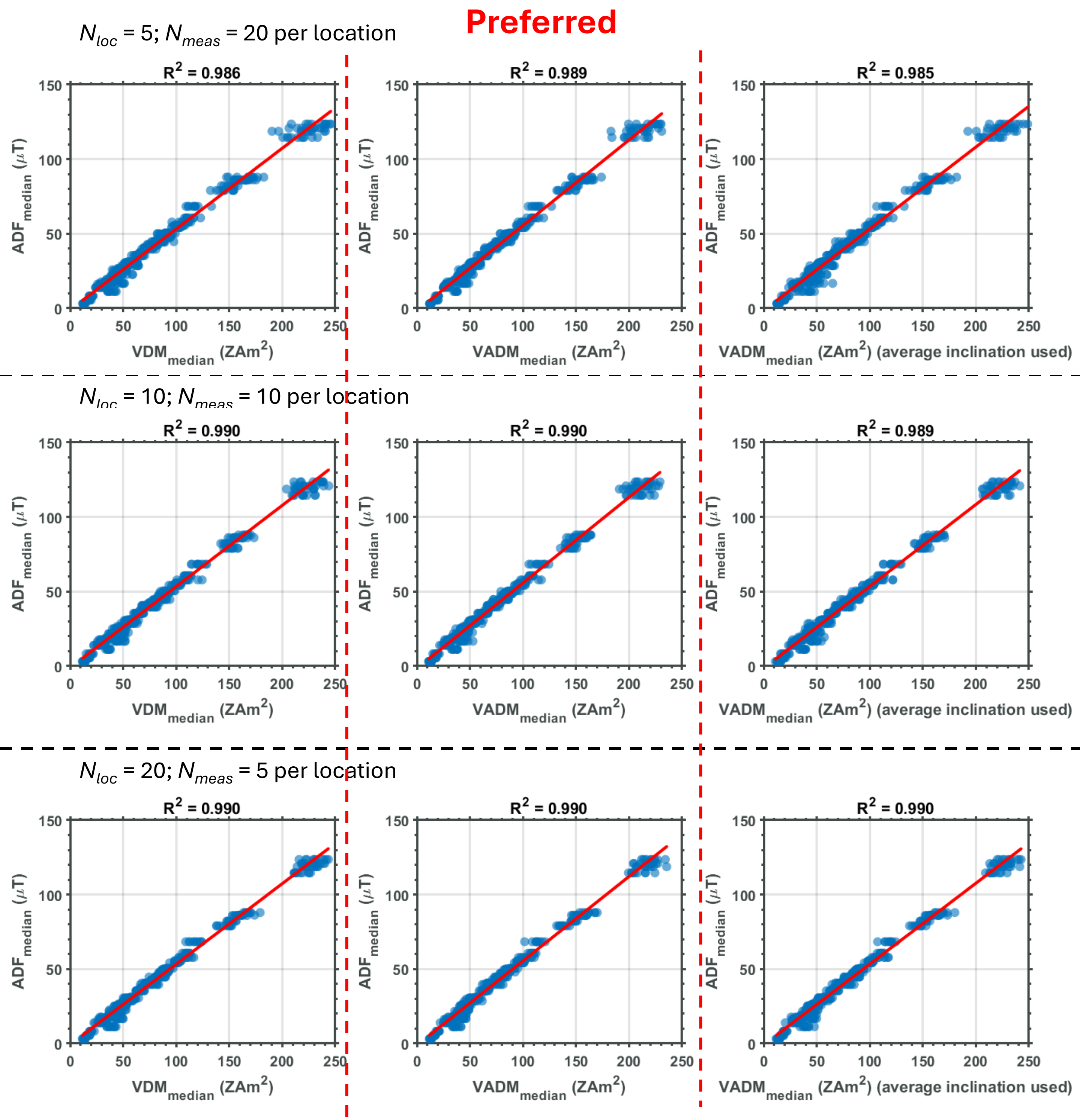

Figure S2: Tests of three palaeomagnetic proxies for ADF_{median} using three different distributions of 100 magnetic field vectors each representing a synthetic palaeomagnetic measurement. Tests were performed using time series of Gauss coefficients produced by our ensemble of geodynamo simulations. Each point on a plot is the median of 100 magnetic field vectors drawn from N_{meas} random timesteps at each of N_{loc} uniformly-distributed locations on the Earth's surface. This was repeated 10 times for each simulation with the absolute locations of the locations randomly determined for each. The proxies are median VDM (left column), median VADM calculated using the geographic latitude (central column; the preferred option) and median VADM calculated using the average inclination at each location (right column). The three rows represent different distributions of the 100 measurements.

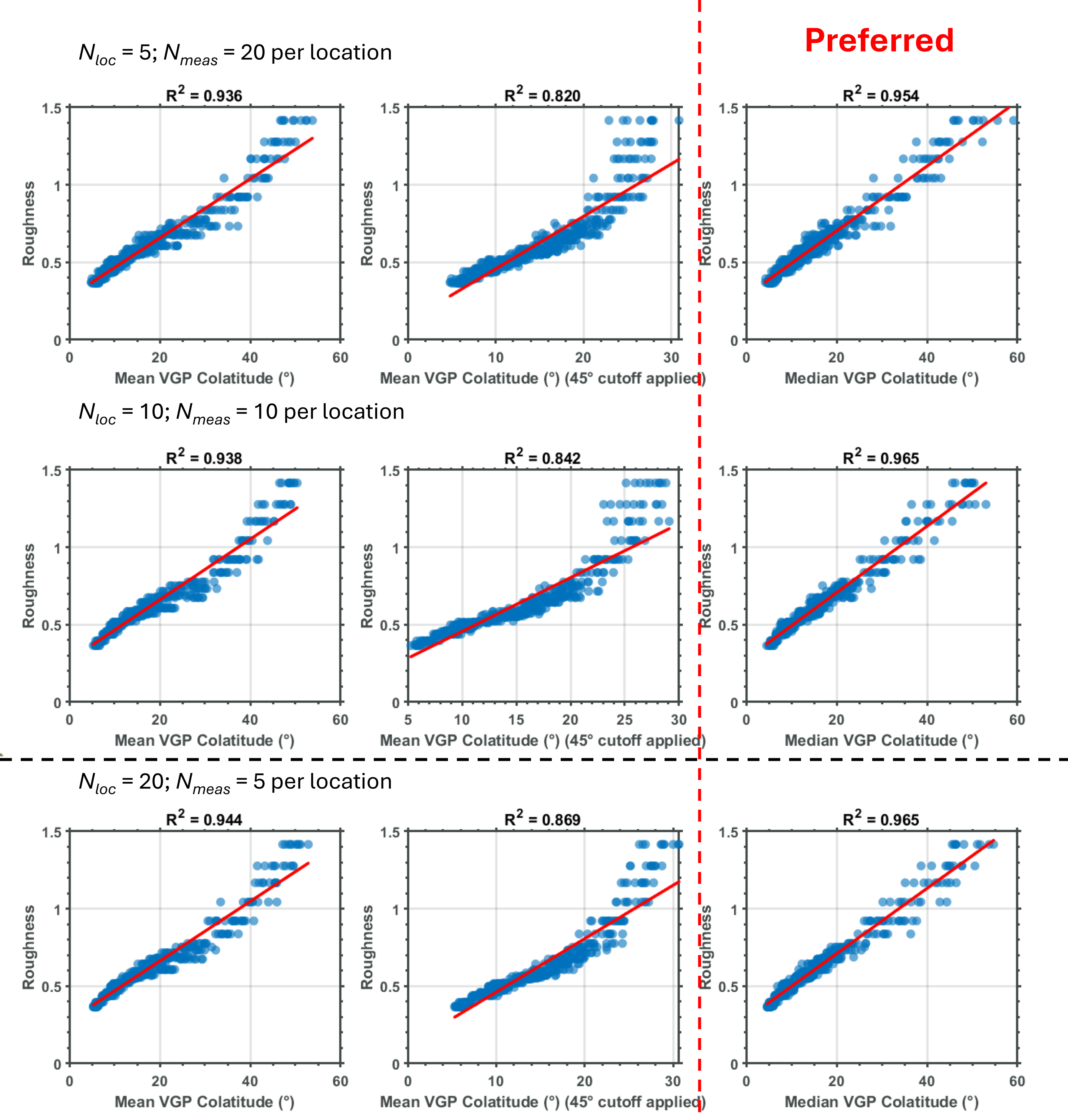

Figure S3: Tests of three palaeomagnetic proxies for *Roughness* using three different distributions of 100 magnetic field vectors each representing a synthetic palaeomagnetic measurement. Tests were performed using time series of Gauss coefficients produced by our ensemble of geodynamo simulations. Each point on a plot is the median of 100 magnetic field vectors drawn from N_{meas} random timesteps at each of N_{loc} uniformly-distributed locations on the Earth's surface. This was repeated 10 times for each simulation with the absolute locations of the locations randomly determined for each. The proxies are mean VGP colatitude (left column), mean VGP colatitude calculated after excluding those larger than 45° (central column) and median VGP colatitude (right column; the preferred proxy). The three rows represent different distributions of the 100 measurements.

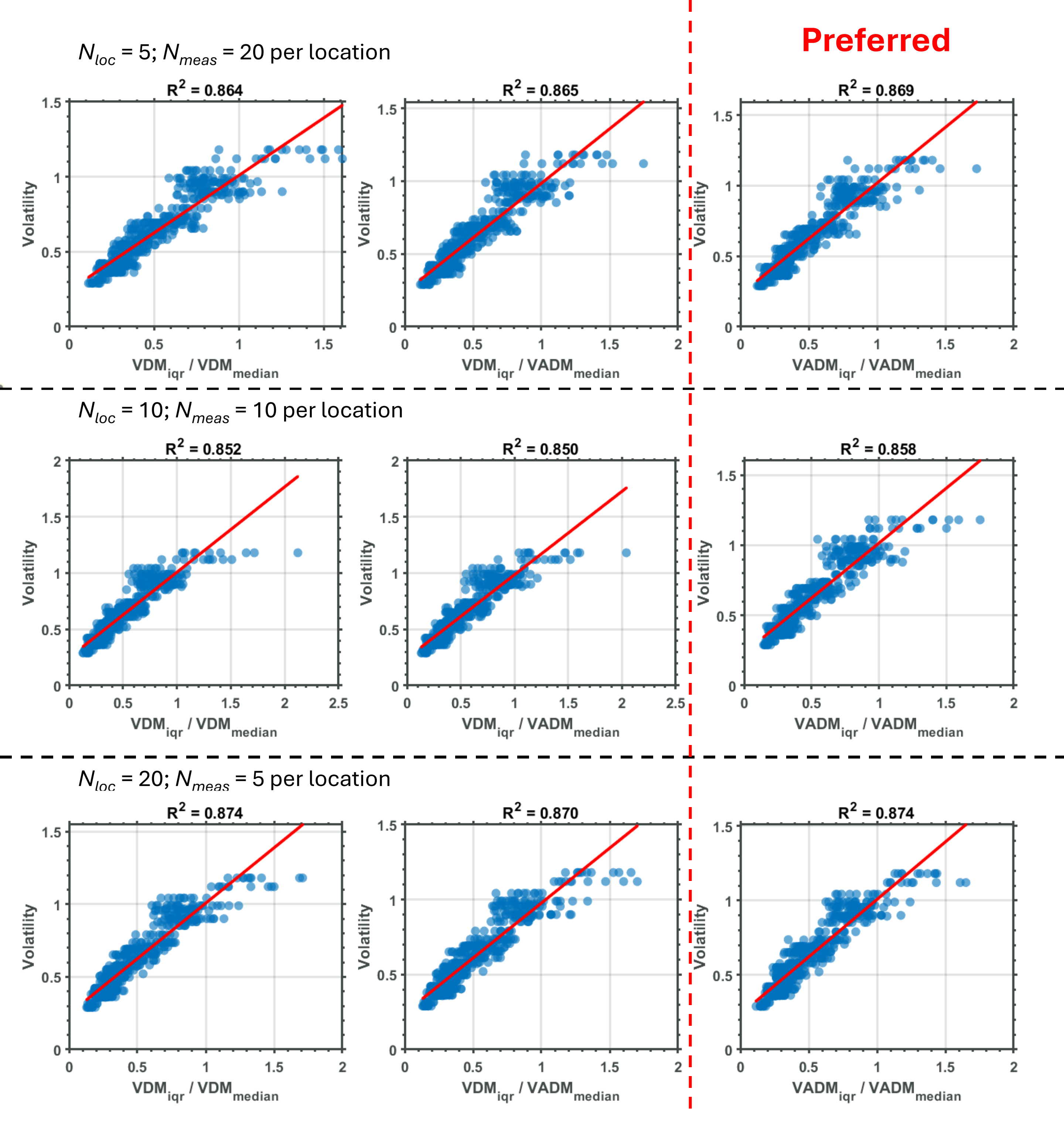

Figure S4: Tests of three palaeomagnetic proxies for *Volatility* using three different distributions of 100 magnetic field vectors each representing a synthetic palaeomagnetic measurement. Tests were performed using time series of Gauss coefficients produced by our ensemble of geodynamo simulations. Each point on a plot is the median of 100 magnetic field vectors drawn from N_{meas} random timesteps at each of N_{loc} uniformly-distributed locations on the Earth's surface. This was repeated 10 times for each simulation with the absolute locations of the locations randomly determined for each. The proxies are median VDM (left column), median VADM calculated using the geographic latitude (central column) and median VADM calculated using the average inclination at each location (right column; the preferred proxy). The three rows represent different distributions of the 100 measurements.

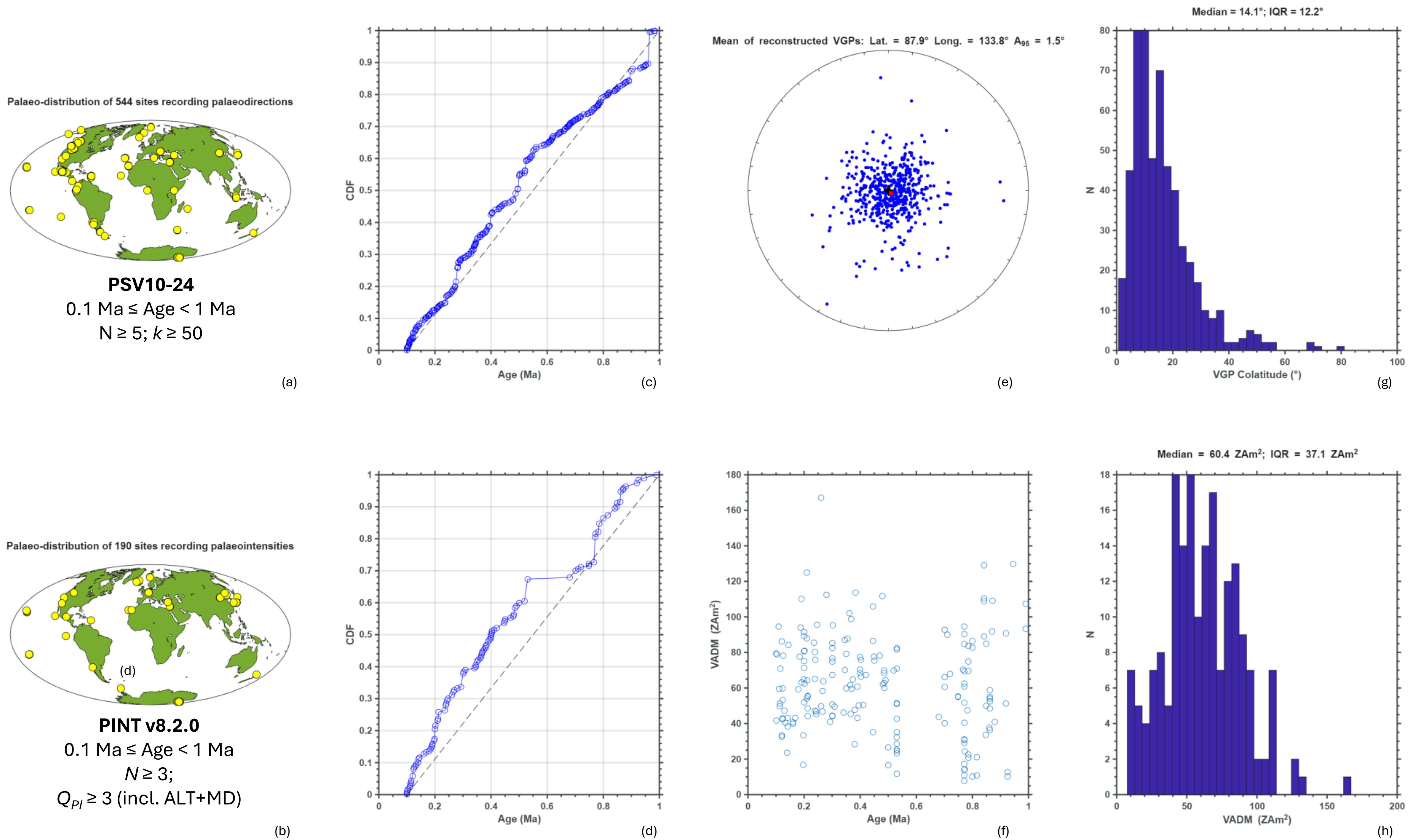

Figure S5: Summary of palaeomagnetic directions (top row) and intensities (bottom row) for time interval 0.1 – 1 Ma. (a,b): Map of distribution of sites after relocation (present-day positions of continents retained); (c,d) Cumulative distributions of ages of data with ideal uniform shown as dashed line; (e) Equal area plot of VGPs after correction for site relocation and declination rotation; (f) Plot of VADM vs Age; (g,h) Histograms of VGP colatitudes and VADMs with summary statistics given.

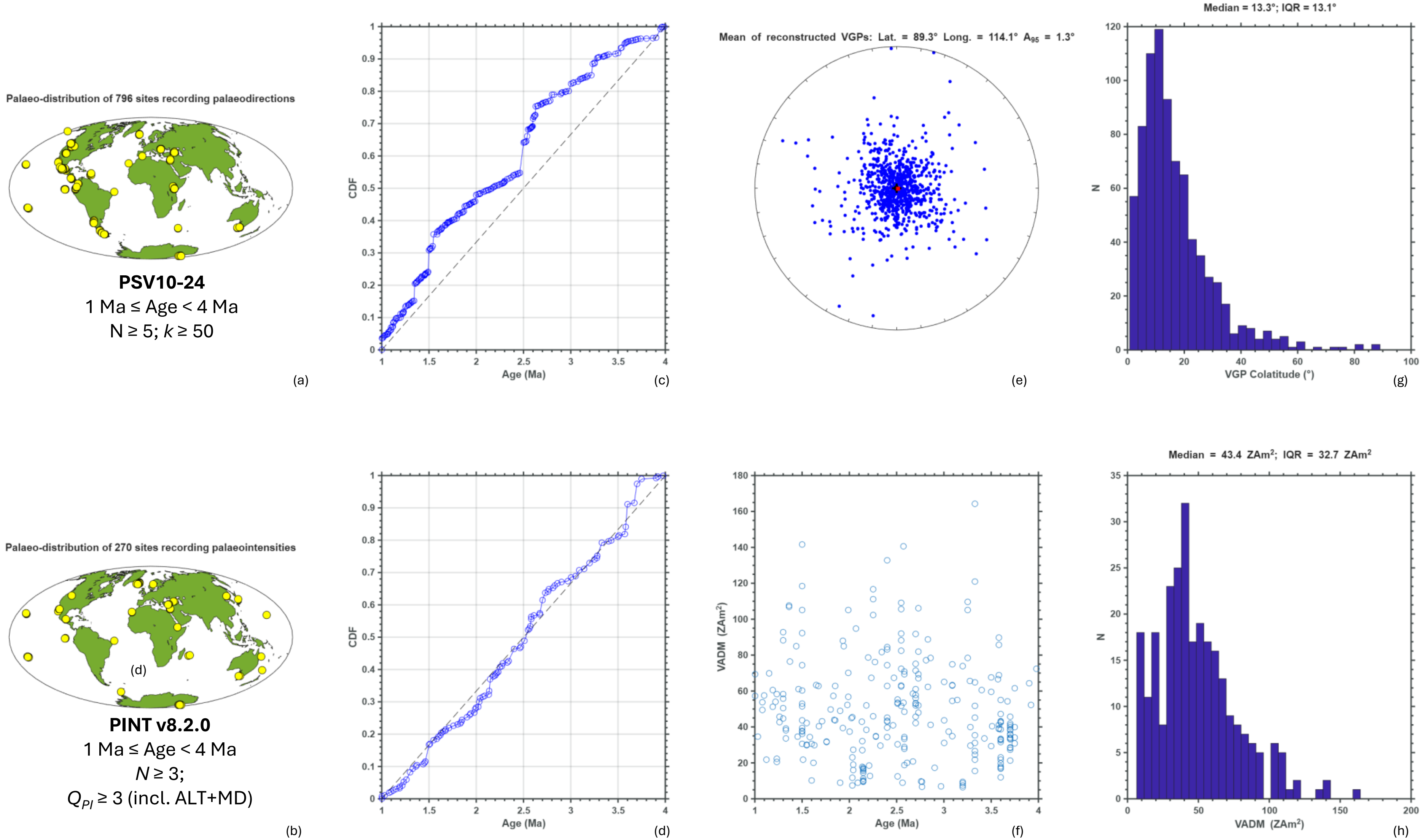

Figure S6: Summary of palaeomagnetic directions (top row) and intensities (bottom row) for time interval 1 – 4 Ma. (a,b): Map of distribution of sites after relocation (present-day positions of continents retained); (c,d) Cumulative distributions of ages of data with ideal uniform shown as dashed line; (e) Equal area plot of VGPs after correction for site relocation and declination rotation; (f) Plot of VADM vs Age; (g,h) Histograms of VGP colatitudes and VADMs with summary statistics given.

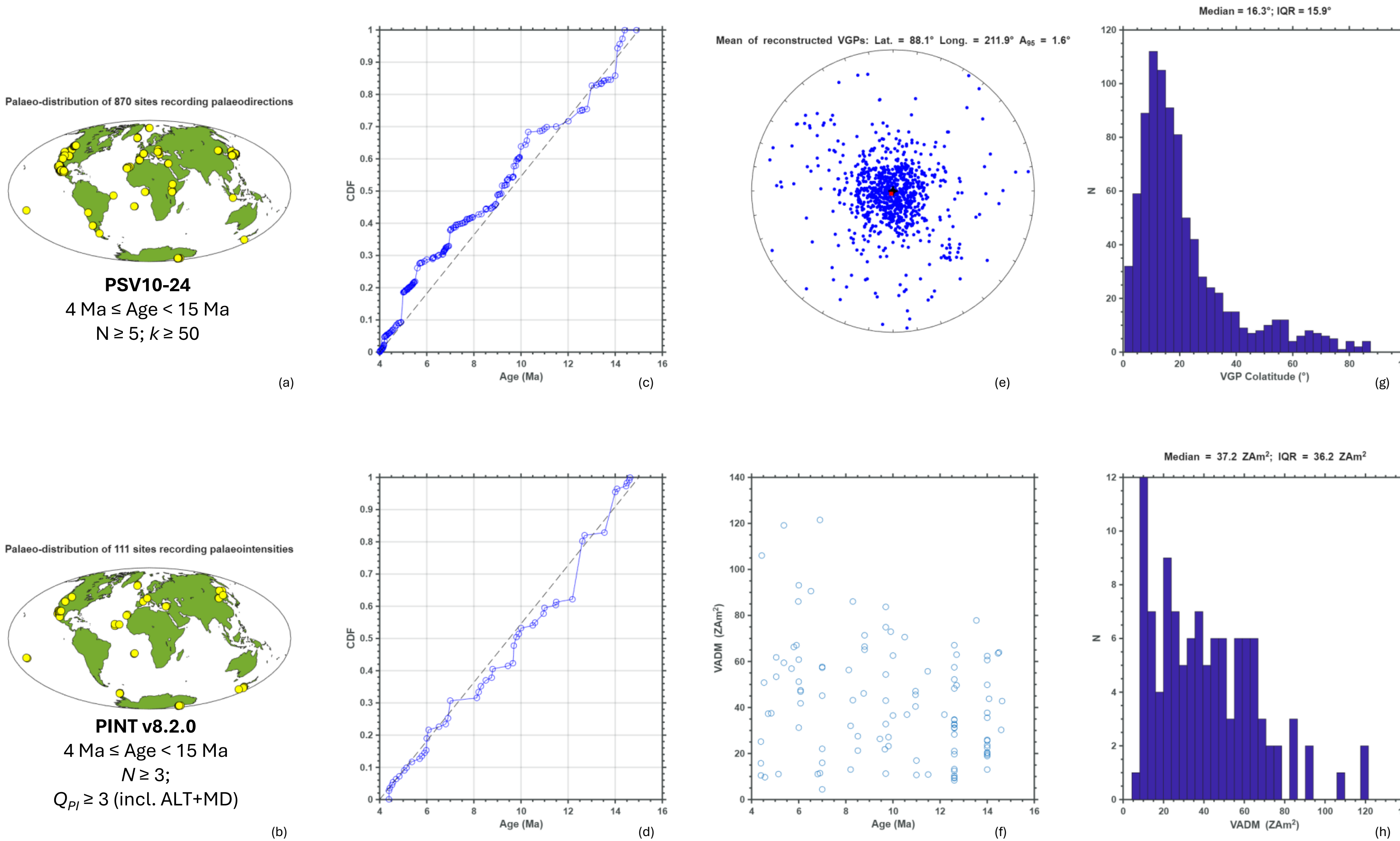

Figure S7: Summary of palaeomagnetic directions (top row) and intensities (bottom row) for time interval 4 - 15 Ma. (a,b): Map of distribution of sites after relocation (present-day positions of continents retained); (c,d) Cumulative distributions of ages of data with ideal uniform shown as dashed line; (e) Equal area plot of VGPs after correction for site relocation and declination rotation; (f) Plot of VADM vs Age; (g,h) Histograms of VGP colatitudes and VADMs with summary statistics given.

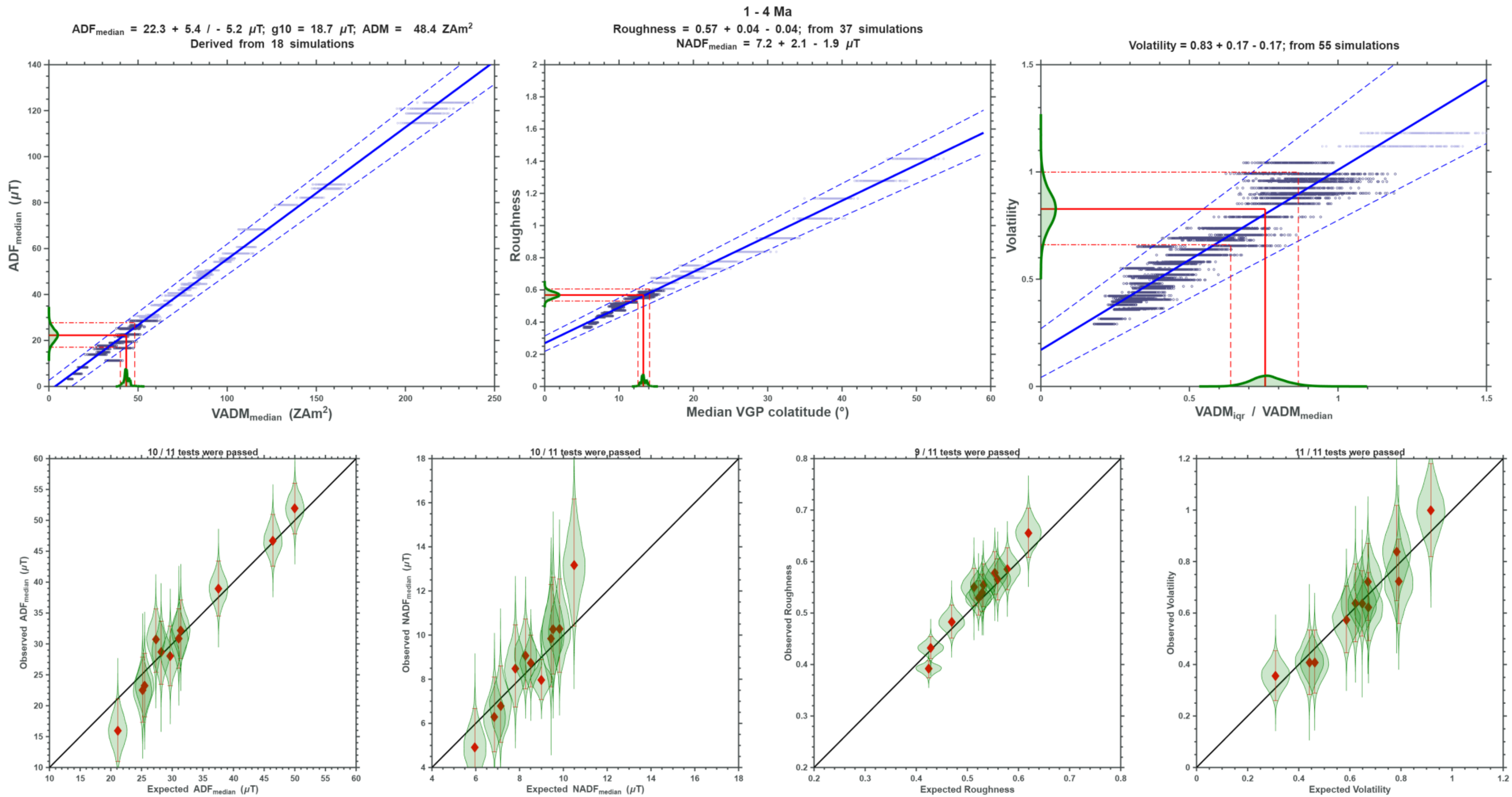

Figure S8: SHAnalogue estimation and testing for the 0.1-1 Ma time interval. (a-c): Bespoke proxy plots derived from outputs of geodynamo simulations down-sampled randomly in time at the spatial resolution of the palaeomagnetic datasets. Each horizontal row of blue points represents 200 proxy values (plotted on x-axis) calculated from a simulation with a single "true" SHAnalogue value (plotted on y-axis). Darker coloured points were used in the estimation of the SHAnalogues from the palaeomagnetic proxies. Vertical red lines indicate the palaeomagnetic proxy central values (solid) and 95% uncertainties (dashed). Horizontal red lines are the corresponding palaeomagnetic SHAnalogue estimates (see text for details of calculation). The shapes of the distributions (amplitudes are arbitrary) of both are shown in green. (d-g) One-to-one plots of the expected and estimated SHAnalogues obtained after down-sampling the 11 geomagnetic field models at the resolution of the 0.1-1 Ma datasets and subjecting these synthetic measurements to the same process as shown in upper panels. The estimates and 95% uncertainties are shown in red while violin plots in green show the shapes of the distributions using arbitrary, relative amplitudes.

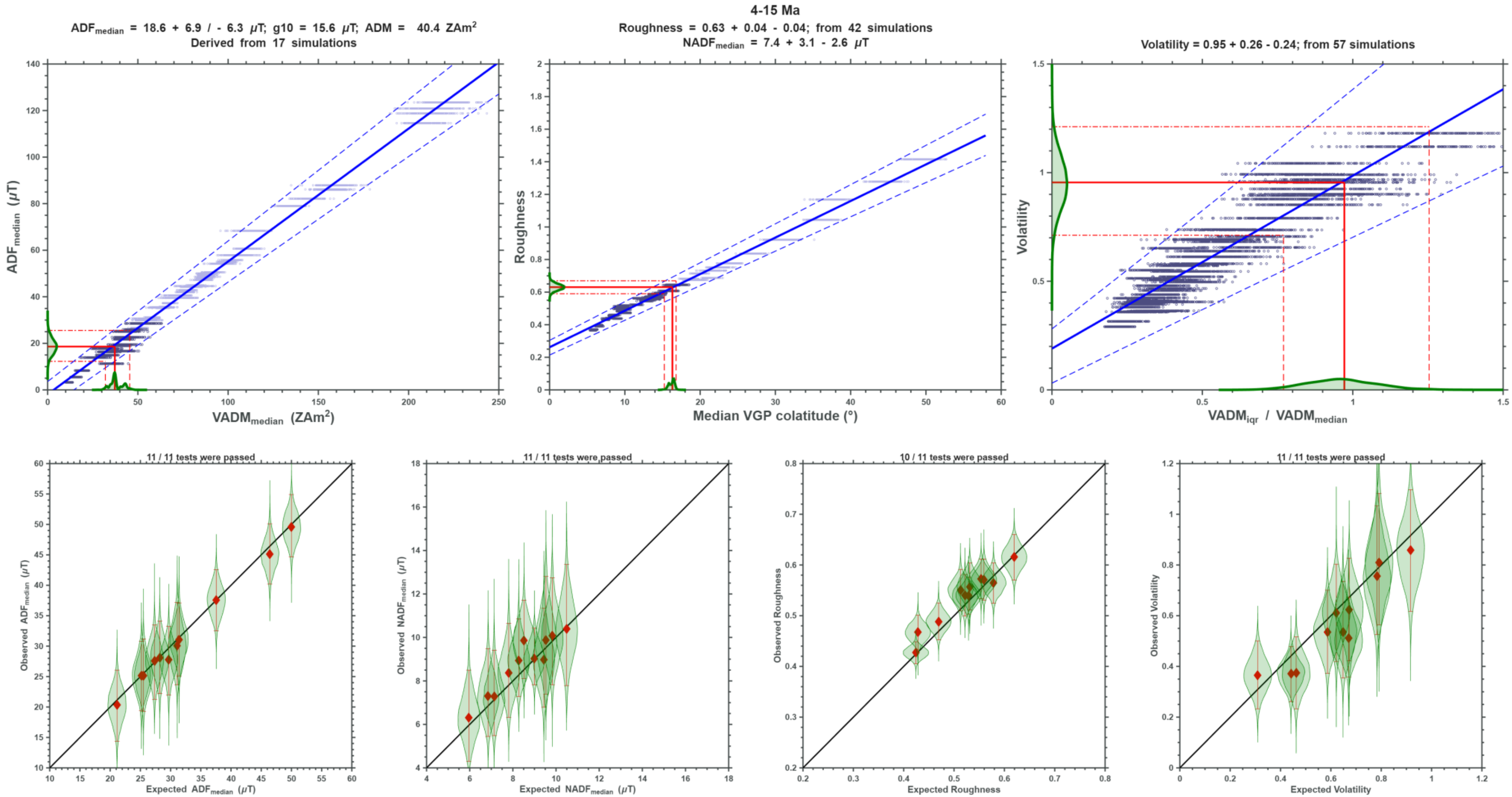

Figure S9: SHAnalogue estimation and testing for the 4-15 Ma time interval. (a-c): Bespoke proxy plots derived from outputs of geodynamo simulations down-sampled randomly in time at the spatial resolution of the palaeomagnetic datasets. Each horizontal row of blue points represents 200 proxy values (plotted on x-axis) calculated from a simulation with a single "true" SHAnalogue value (plotted on y-axis). Darker coloured points were used in the estimation of the SHAnalogues from the palaeomagnetic proxies. Vertical red lines indicate the palaeomagnetic proxy central values (solid) and 95% uncertainties (dashed). Horizontal red lines are the corresponding palaeomagnetic SHAnalogue estimates (see text for details of calculation). The shapes of the distributions (amplitudes are arbitrary) of both are shown in green. (d-g) One-to-one plots of the expected and estimated SHAnalogues obtained after down-sampling the 11 geomagnetic field models at the resolution of the 0.1-1 Ma datasets and subjecting these synthetic measurements to the same process as shown in upper panels. The estimates and 95% uncertainties are shown in red while violin plots in green show the shapes of the distributions using arbitrary, relative amplitudes.

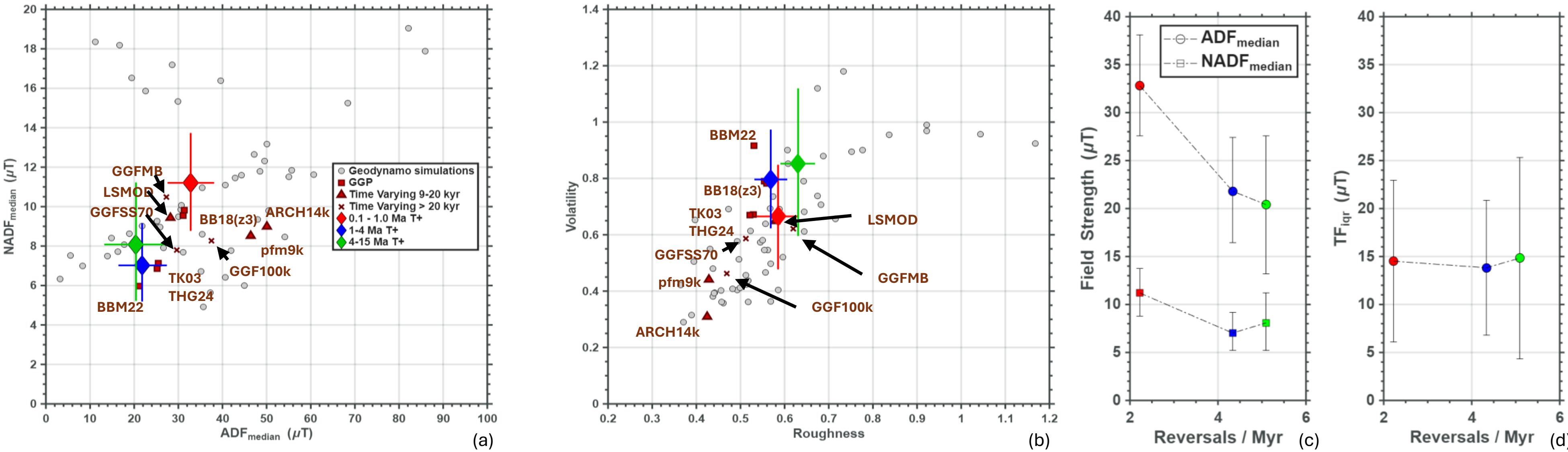

Time period	N_{dir}	N_{int}	ADF_{median} (μT)	$NADF_{median}$ (μT)	*Roughness*	*Volatility*	Test Success
0.1-1 Ma	544	120	33 ± 5	11 +3 / -2	0.59 ± 0.05	0.67 + 0.18 /-0.19	98%
1-4 Ma	796	194	22 +6 / -5	7 ± 2	0.57 ± 0.04	0.80 +0.18 / -17	93%
4-15 Ma	870	90	20 ± 7	8 ± 3	0.63 ± 0.04	0.85 + 0.27 /-0.26	98%

(e)

Figure S10: Summary of SHAnalogue estimation and averaged polarity reversal frequency for the time periods 0.1-1 Ma, 1-4 Ma, and 4-15 Ma using only palaeointensities derived using, in part, the Thellier method with pTRM checks. (a,b) Plot of ADF_{median} vs. $NADF_{median}$ and *Roughness* vs. *Volatility* with direct measurements from geomagnetic field models and geodynamo simulations also shown. (c) Plots of ADF_{median} and $NADF_{median}$ vs. polarity reversal rate. (d) Plot of TF_{iqr} (derived from $Volatility^2$. ADF_{median}) vs. polarity reversal rate. All error bars indicate 95% uncertainty bounds. (e) Tabulated summary of results.